Design and Cyclic Experiments of a Mass Timber Frame with a Timber Buckling Restrained Brace

Emily Williamson, S.M.ASCE[1]; Chris P. Pantelides, F.ASCE[2]; Hans-Erik Blomgren, M.ASCE[3]; and Douglas Rammer, M.ASCE[4]

Abstract: Mass timber buildings are increasing in popularity as the building industry aims to use more sustainable construction materials. A lateral force resisting system with a mass timber frame and a timber buckling restrained brace (TBRB) is presented as a possible solution to allow the expanded use of mass timber in buildings located in cities with high risk of natural hazards such as earthquakes and hurricanes. A series of nine quasi-static cyclic tests was completed to study the performance of the TBRB frame as well as the elastic performance of the bare mass timber frame. The variables studied included the level of axial force applied to the columns to simulate gravity load and the out-of-plane displacement of the TBRB frame. The mass timber frame was tested four times with a different TBRB. The four subassemblies achieved a drift ratio of at least 2.8% before failure of the TBRB due to weak axis buckling of the steel core. The maximum displacement ductility of the four TBRB frame subassemblies ranged from 3.1 to 3.5. The addition of the TBRB enhanced the energy dissipation capacity of the bare mass timber frame by 4.0 to 8.6 times after 14 cycles of lateral displacement. **DOI: 10.1061/JSENDH.STENG-12363.**

Author keywords: Mass timber; Buckling-restrained brace; Mass ply lam frame; Dowel connections; Cyclic; Ductility; Earthquakes.

Introduction

The benefits of mass timber have led the building industry, including developers, architects and engineers to promote construction of mass timber buildings. Benefits of mass timber construction include cost savings in foundations due to timber's light weight, decreased construction time caused by prefabrication, sustainable characteristics, and architectural appeal. Engineered timber products including glued laminated timber, laminated veneer lumber (LVL), cross laminated timber (CLT), dowel laminated timber (DLT), nail laminated timber (NLT), laminated strand lumber (LSL), and parallel strand lumber (PSL) allow engineers to take advantage of these benefits because the materials are manufactured with sorted layers of the strongest, most ideal parts of a tree. Mass ply panel (MPP) and mass ply lam (MPL), respectively (APA 2022), are constructed by pressing together 25 mm (1-in.) LVL laminations with varying cross-grain orientations. The layup of the MPL and MPP presents advantages compared to other engineered timber materials. MPL and MPP perform as if self-reinforced against tension perpendicular-to-grain forces because the cross-ply veneers within each lamination provide increased stiffness and additional dimensional stability.

The first tall wood buildings were built in Europe and Canada as code alternative solutions. In 2015, the United States ICC Ad Hoc Committee for tall wood structures developed new code language for tall wood structures that was incorporated in the 2021 IBC (ICC 2021). A main challenge for adopting mass timber as the primary structural material is the lack of defined timber lateral force resisting systems (LFRS) in building codes. Current building codes do not define overstrength (Ω), deflection amplification (C_d), and response modification (R) factors for timber braced frames; hence, tall timber buildings are typically built with a mass timber gravity system and a steel or concrete core LFRS. This hybrid approach can lead to added costs due to custom connection details required to accommodate tolerances between materials, and more construction trades present on the site that leads to increases in construction time.

One well-defined mass timber LFRS is the mass timber shear wall. Mass timber walls are quite rigid, so care must be taken to develop proper wall base connections to take full advantage of the wall strength (Morrell et al. 2020; Popovski and Gavric 2015). Studies have been completed to evaluate the seismic performance of CLT shear walls, with two generic connection types, and to determine the corresponding Ω, C_d and R factors (van de Lindt et al. 2020, 2022). Rocking walls using post-tensioning achieve high drift ratios with self-centering, but experience significant damage to the base of the wall (Ganey et al. 2017). Post-tensioned mass timber rocking walls have been tested successfully in mass timber building shake table tests (Pei et al. 2019); furthermore, seismic design procedures for post-tensioned mass timber rocking walls have been developed (Busch et al. 2021). Slip friction joints (RSFJ) are an alternative solution for decreasing residual drift and floor accelerations in timber buildings (Fitzgerald et al. 2020; Hashemi et al. 2017). Perforated steel plates have been used as energy dissipators in CLT shear walls as panel connectors or hold-downs (Daneshvar et al. 2022a, b). Finally, Lo Ricco et al. (2021) illustrated the design process for a building with self-centering rocking CLT shear walls using the equivalent lateral force procedure.

[1]Graduate Research Assistant, Dept. of Civil and Environmental Engineering, Univ. of Utah, Salt Lake City, UT 84112. ORCID: https://orcid.org/0000-0003-0927-0771. Email: emily.diedrich@utah.edu

[2]Professor, Dept. of Civil and Environmental Engineering, Univ. of Utah, Salt Lake City, UT 84112 (corresponding author). ORCID: https://orcid.org/0000-0003-3309-3488. Email: c.pantelides@utah.edu

[3]Structural Engineer, Timberlab, 1601 NE Columbia Blvd., Portland, OR 97211. Email: hans-erik.blomgren@timberlab.com

[4]Research Engineer, Forest Products Laboratory, One Gifford Pinchot Drive, Madison, WI 53726. Email: douglas.r.rammer@usda.gov

Note. This manuscript was submitted on December 28, 2022; approved on May 30, 2023; published online on July 26, 2023. Discussion period open until December 26, 2023; separate discussions must be submitted for individual papers. This paper is part of the ***Journal of Structural Engineering***, © ASCE, ISSN 0733-9445.

Timber braced frames present an alternative for mass timber LFRS, but these types of frames have limited drift and energy dissipation capacity due to the brittle nature of timber braces (Cao et al. 2021). Popovski et al. (2003) noted that the variability of the wood used to manufacture elements such as glulam braces can lead to a nonuniform response of the two brace ends. Moreover, timber frames rely on the connections to provide ductility and energy dissipation. Xiong and Liu (2014) performed monotonic and cyclic tests on glulam frames with bolted connections and found that X-brace and K-brace configurations experienced brittle failure modes caused by tension in the braces and failure at the connections. One drawback of timber connections is the tendency to prematurely fail because of splitting caused by tension perpendicular to grain. Providing additional screw reinforcement improves the ductility of dowel and bolted connections (Dietsch and Brander 2015; Dong et al. 2021; Min-juan and Hui-fen 2015; Zhang et al. 2019). There have been studies regarding different types of timber connections including glulam rivets (Popovski et al. 2001), and glued in rods (Steiger et al. 2015; Otero-Chans et al. 2018).

There has been work to improve the performance of mass timber frames to avoid the significant damage to connections caused by large drift demands, which requires them to be replaced. Gilbert and Erochko (2019) tested a steel beam-column brace joint with glued in rods to determine if the connection could allow timber buildings to use the same R values used in steel frames with high performance dampers. Hashemi et al. (2021) and Yousef-beik et al. (2020) presented a mass timber braced frame with RSFJs at the ends and at the middle of the brace, respectively, to protect the joints from damage and provide energy dissipation capability within the brace; a similar study was conducted by Daneshvar et al. (2022a), who tested braces with perforated plates at the ends as the energy dissipating element.

A popular LFRS for steel buildings in high seismic zones is the buckling restrained brace frame (BRBF). The conventional buckling-restrained brace (BRB) is constructed using a steel yielding core encased in a concrete-filled steel tube. The steel tube restrains the core to prevent global buckling, thus allowing it to have a uniform response in tension and compression. The conventional BRB has been tested extensively; it has a stable hysteresis curve with no pinching, thus allowing higher energy dissipation compared with other types of steel braces (Black et al. 2004; Fahnestock et al. 2007; Wu et al. 2014; Xu and Pantelides 2017).

Researchers have been working to develop a ductile lateral force resisting system for mass timber buildings using conventional BRBs. Dong et al. (2020) tested a glulam frame with two conventional BRBs in a chevron configuration; two full-scale frames with different connection types were built; the frames achieved 1.5% story drift ratio before the tests were terminated due to actuator limitations. The BRB glulam frames were able to achieve a displacement ductility of 2.3 to 2.8 using the equivalent energy elastic-plastic (EEEP) method (ASTM 2011).

Murphy et al. (2021) completed component tests of six TBRBs under high strain and fatigue loading protocols; the full-scale TBRBs were 3.66 m (12 ft) long and were designed for a 267 kN (60 kip) yield capacity. These component tests showed that the TBRB, which uses similar design principles as the conventional BRB is able to meet or surpass the standards set by AISC 341-16 (AISC 2016), thus presenting a promising mass timber LFRS solution.

This paper discusses the design and testing of a mass timber frame with a TBRB, termed a TBRBF. Four TBRBs were tested with two levels of column axial force; two in-plane and two out-of-plane tests were carried out. In addition, the bare mass timber frame was tested in the elastic range before each TBRBF test to determine the initial stiffness of the frame and observe potential stiffness degradation with each subsequent test.

Mass Timber Frame Design

The frame designed for the tests represents a two-thirds scale single-bay braced frame in a mass timber building with a single diagonal (zig-zag) configuration [Fig. 1(a)]. The columns extend below the bottom beam to ensure the expected frame action could occur during the tests. The column center-to-center spacing was 3.05 m (120 in.) and the story height was 2.29 m (90 in.). The frame was designed for the adjusted forces of a 178 kN (40 kip) TBRB following the capacity design approach for beams, columns, and connections in a conventional BRBF. The material properties and dimensions for the components of the frame are included in Table 1.

Timber BRB

As described in Murphy et al. (2021), the TBRB is designed following similar principles as set by AISC 341-16 (AISC 2016) for conventional steel-concrete BRBs. The nonyielding members of the TBRB frame are designed for the expected BRB forces based on brace properties and adjustment factors. The compression adjustment factor, β, is defined as the ratio of maximum compression to tension force; the strain hardening adjustment factor, ω, is defined as the ratio of maximum force achieved in tension to the tension yield force. According to conventional BRB requirements, β must be greater than 1.0 but less than 1.5 and ω must be greater than 1.0. The expected maximum force in tension, $T_{\max}$, is calculated with Eq. (1) and the expected maximum force in compression, $C_{\max}$, is calculated with Eq. (2)

$$T_{\max} = \omega R_y F_y A_{sc} \tag{1}$$

$$C_{\max} = \beta\omega R_y F_y A_{sc} \tag{2}$$

where R_y = ratio of expected to specified yield stress, F_y = steel core specified yield stress, and A_{sc} = cross-sectional area of the yielding portion of the steel core. The connections and connecting members are designed to withstand the force that results in the highest demand.

The TBRBs for this frame were designed to have an axial yield force of 178 kN (40 kips) based on the fact that the timber frame was a two-thirds scaled model. To achieve this strength, the core was specified to be 276 MPa (40 ksi) steel; coupon tests of the steel core determined the true yield strength of the steel, specified in Table 1. The steel core was designed with the dimensions shown in Fig. 2(a); the yielding zone was 13 mm (½ in.) thick by a 51 mm (2 in.) wide. The casing consisted of two 254 mm (10 in.) by 152 mm (6 in.) F10 MPP (APA 2022) elements oriented so that the X-direction of the member, according to ASTM D5456 (ASTM 2019), was perpendicular to the steel core. A hardwood spacer, shown in Figs. 2(a and c), was screwed in place on the sides of the steel core to fill the void between the casing and prevent strong axis buckling of the core; 13 mm (½ in.) diameter mild steel threaded rods along the yielding portion of the core and 6 mm (1/4 in.) diameter threaded rods near the two ends, with the properties specified in Table 1, held the assembly together.

The desired performance of the TBRB requires that failure occurs within the yielding zone of the steel core. To achieve this, the stiffness at the ends of the steel core plate was increased by welding 38 mm (1½ in.) wide by 13 mm (½ in.) thick stiffeners and 6 mm (1/4 in) cheek plates to either side of the core. In addition, a 25 mm

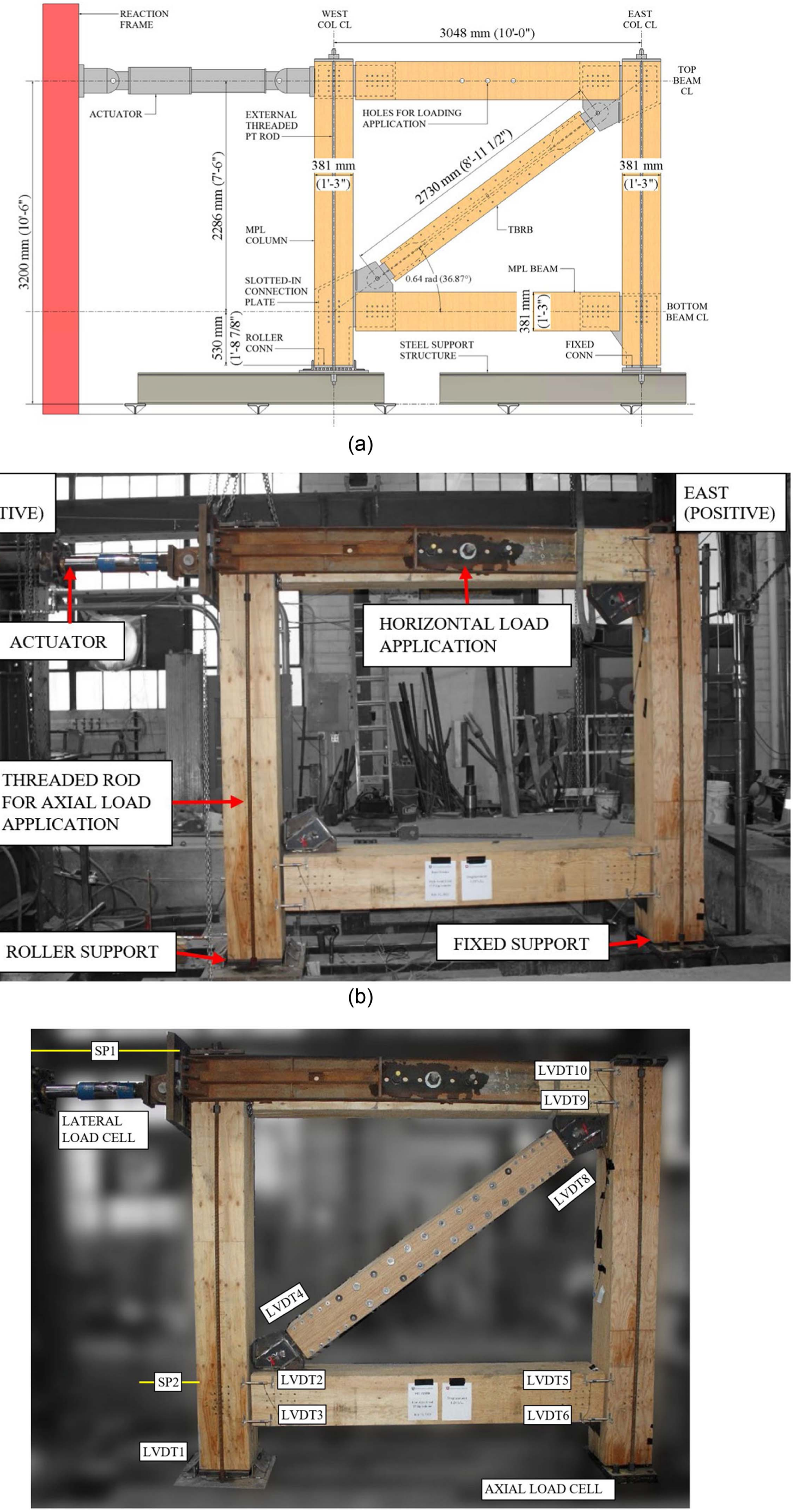

Fig. 1. TBRB frame testing configuration: (a) dimensions; (b) bare frame; and (c) TBRBF.

J. Struct. Eng., 2023, 149(10): 04023131

Table 1. Component dimensions and material properties

Component	Dimensions	Material properties
Beams and columns	Width = 389 mm (15 − 5/16 in.) Depth = 381 mm (15 in.)	F16 MPL[a] E = 11 GPa (1,600 ksi)
Dowels	Diameter = 13 mm (½-in.) Length = 381 mm (15 in.)	F_y = 248 MPa (36 ksi)
Connection plates	Thickness = 13 mm (½-in.)	F_y = 248 MPa (36 ksi)
TBRB steel core	Yielding zone = 1,549 mm (61 in.) 13 mm × 51 mm (1/2 in. × 2 in.) Ends 13 mm × 178 mm (1/2 in. × 7 in.)	F_y = 262 MPa (38 ksi)
TBRB casing	254 mm × 152 mm × 2,426 mm (10 in. × 6 in. × 95.5 in.)	F10 MPP[a] E = 6,206 MPa (900 ksi)
TBRB threaded rods	Yielding zone 13 mm × 356 mm (½ in. × 14 in.) Ends 6 mm × 356 mm (¼ in. × 14 in.)	F_y = 634 MPa (92 ksi) F_y = 634 MPa (92 ksi)

[a]Data from APA (2022).

(1 in.) diameter by 76 mm (3 in.) steel dowel was welded to the center of the core and embedded into the MPP casing to help distribute the brace forces evenly and keep the casing centered on the steel core plate.

Beam-Column-Brace Connections

Similar to the design of a steel frame with a conventional BRB, the beam-column connections were designed with a capacity-based approach. Each connection was designed for the adjusted forces of a 178 kN (40-kip) TBRB using Eqs. (1) and (2). The compression adjustment factor, β, and strain hardening factor, ω, were 1.25 and 1.45, respectively based on the results from Murphy et al. (2021). The value of R_y was 1.0 since coupon tests were performed to determine the true tensile yield stress of the steel core. The beam-column connections shown in Figs. 2(d–g) were designed using equations for dowel connections defined by the National Design Specification for Wood Construction (AWC 2018a), NDS technical report (AWC 2018b), and an equivalent model for connections with multiple slotted-in steel plates (Fan et al. 2011). Williamson et al. (2023) describes the design process and testing of connections similar to the ones used in the mass timber frame; based on the experimental results, the connections were expected to achieve adequate rotation without additional joint reinforcing. Each connection included two slotted-in steel plates and smooth shank steel dowels [Fig. 2(d)]; the properties of these components are included in Table 1. The slots and holes were cut using a computer numerical controlled (CNC) machine to meet construction tolerances. A 25 mm (1 in.) gap was left between the beam ends and the face of the column to allow for member rotation without contact between members.

At the beam-column-brace connections, the steel plates were extended beyond the timber members to form gusset plates for the TBRB pin connection [Figs. 2(e and f)]; to avoid premature buckling of the gusset plates, they were reinforced with 13 mm (0.5 in.) vertical stiffeners, welded between the gusset plates 25 mm (1 in.) from the face of the column to allow column rotation, and a 6 mm (¼ in.) thick cheek plate in the critical area of the gusset plate to avoid tear out of the pin connection. Steel spacers were placed around the pin between the steel core end and gusset plate to limit out-of-plane shifting of the core.

Experimental Program

A single mass timber frame was used for the entire testing program. Bare frame tests were performed at the beginning, end, and in-between TBRBF tests to determine the mass timber frame's contribution to the strength of the system and to monitor potential stiffness degradation of the mass timber frame itself with each test. The experimental program, in sequential order, is summarized in Table 2. Four TBRBF tests were completed; two of the tests with no out-of-plane restraints at the top of the frame and two with the upper east corner of the frame intentionally displaced 25 mm (1 in.) out-of-plane. The tests included two levels of column axial force; the low axial force level was equivalent to 5% of the column axial capacity or 120 kN (27 kips) per column; the high axial force level was equivalent to 12% of the column capacity or 300 kN (67.5 kips) per column.

Frame Supports

The test setup is shown in Fig. 1(b) for the bare frame and Fig. 1(c) for the TBRB frame. To simulate the behavior of a frame in a mid-floor of a building, the frame supports were configured to transfer the horizontal force from the brace joint in the west through the bottom MPL beam to the east column base connection. To achieve this, the east column support was fixed [Fig. 2(g)] to the strong floor by extending the connection plates 25 mm (1 in.) beyond the bottom of the timber column and welding them to the steel supports. The west column support was designed as a roller support [Fig. 2(f)]; a steel plate was welded to the steel connection plates at the base of the MPL column, and smooth pins were placed between the steel support and the column base; to limit column base displacement, angle stoppers were welded on the east and west side of the west column base with a gap to limit movement. Two external 25 mm (1 in.) diameter 1,034 MPa (150 ksi) all-threaded bars were used to apply axial force to each column.

Loading Protocol

The lateral loading protocol adopted in this program was ASTM E2126 test method B (ASTM 2011), which defines loading procedures for timber cyclic tests (Fig. 3). The first five steps had a single cycle and were applied at a loading rate of 61 mm/min

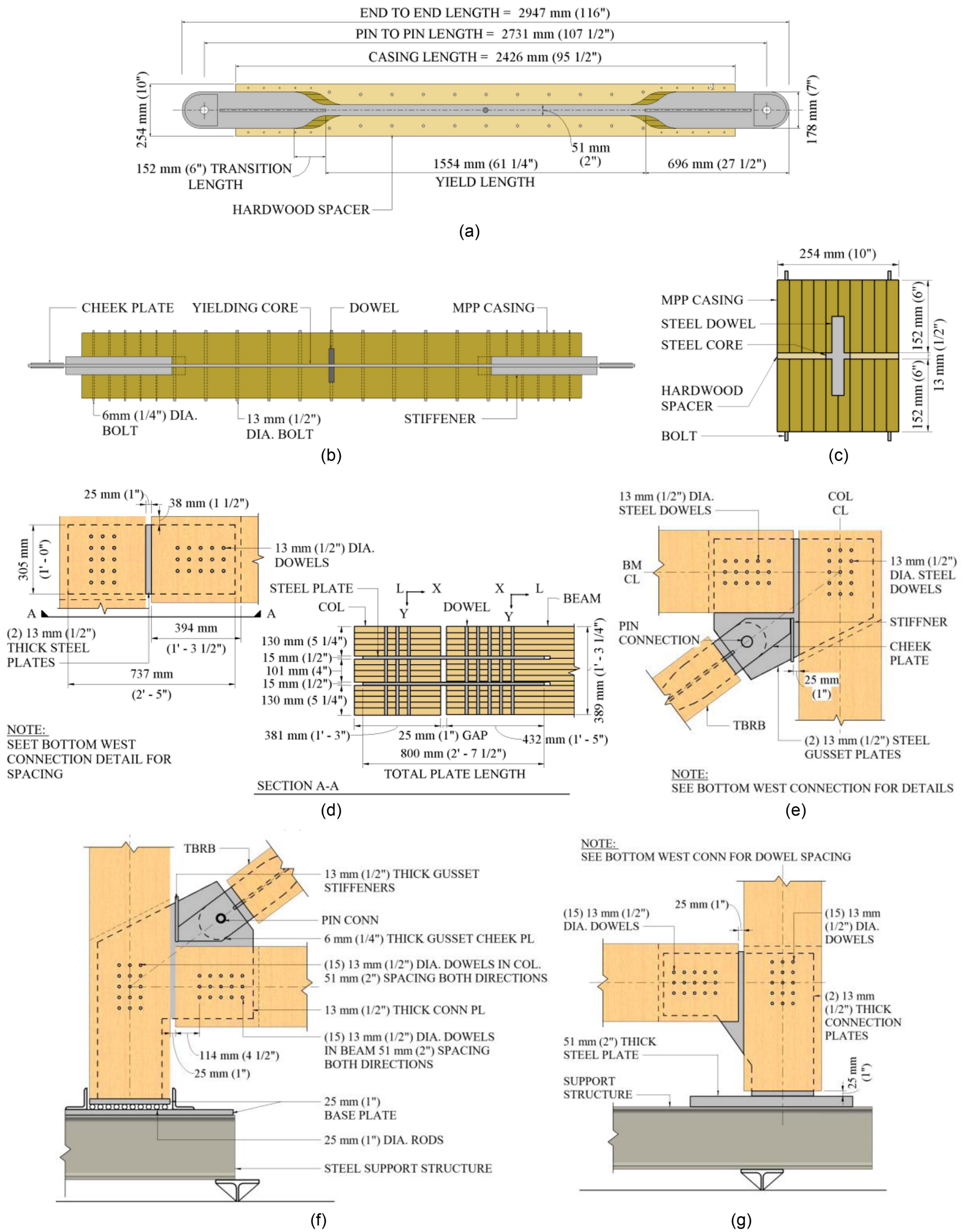

Fig. 2. TBRB and TBRBF connection details: (a) TBRB plan view; (b) TBRB longitudinal section view; (c) TBRB section; (d) top west; (e) top east; (f) bottom west; and (g) bottom east.

Table 2. Test matrix

Test name	Testing configuration	Mass timber frame type	Axial load in each column—kN (kips)
I-BF1	In-plane	Bare	120 (27)
I-BRB1	In-plane	TBRB	120 (27)
I-BF2	In-plane	Bare	300 (67.5)
I-BRB2	In-plane	TBRB	300 (67.5)
O-BF3	Out-of-plane	Bare	120 (27)
O-BRB3	Out-of-plane	TBRB	120 (27)
O-BF4	Out-of-plane	Bare	300 (67.5)
O-BRB4	Out-of-plane	TBRB	300 (67.5)
O-BF5	Out-of-plane	Bare	300 (67.5)

Note: I = in-plane test; and O = out-of-plane test.

(2.4 in./min); the remaining steps were applied at a loading rate of 122 mm/min (4.8 in./min), and the cycle was repeated three times. The displacement is positive when the actuator pushes toward the east column and negative when it pulls away from the west column, as shown in Fig. 1(b). The peaks of each cycle were defined as a percentage of a maximum horizontal actuator displacement (100% Δ_m) corresponding to a maximum theoretical strain of the TBRB achieved in the component tests by Murphy et al. (2021). The bare frame tests were terminated after the 60% Δ_m cycles to limit the structural response to remain within the elastic range of the connections.

Instrumentation

The bare frame and TBRBF tests utilized the same instrumentation plan, as shown in Fig. 1(c). String pots attached to the top (SP1) and bottom beams (SP2) recorded displacements used to calculate the drift. Linear variable displacement transducers (LVDT) were placed near the top and bottom of the beam-column connections to track joint rotation (LVDT 2 to LVDT7). LVDT 8 and LVDT 9 at the TBRB ends were used to measure deformation of the yielding core; LVDT 1 was placed at the base of the west column to track the column displacement at the roller. Each set of gusset plates had one strain gauge attached near the center parallel to the orientation of the TBRB. Load cells at each external threaded bar measured the column axial force. For the tests with intentional out-of-plane displacement, additional string pots were attached to the top of the east column parallel and perpendicular to the frame.

Experimental Results

The results are presented with respect to the drift ratio of the mass timber frame, that is the relative displacement between the top and bottom beam centerlines in Fig. 1(a), equal to SP1 minus SP2 in Fig. 1(c), divided by the vertical height between them equal to 2,286 mm (90 in.).

Hysteresis Curves

The bare mass timber frame cyclic tests were terminated at a drift ratio of 2.0% to ensure the connections remained elastic so as to maintain integrity of the frame. Moreover, the bare frame tests were completed as intermediate steps for monitoring the condition of the frame. The narrow hysteresis loops in Fig. 4 indicate that the frame remains mostly elastic during the bare frame tests; this provides context for understanding the effectiveness of the TBRB energy dissipation capabilities, as well as the TBRB contribution to the strength of the system. At a 2.0% drift ratio the TBRBF resisted 3.0 to 3.8 times the lateral load of the bare mass timber frame.

Test I-BRB1 [Fig. 5(a)] was stopped following completion of the second 100% Δ_m cycle; high amplitude weak axis buckling of the steel core near the west end of the yielding zone caused splitting of the MPP casing between laminas resulting in a 107.6 kN (24.2 kip) drop in lateral load. I-BRB2 [Fig. 5(b)] began splitting in the first 100% Δ_m cycle on the east end of the yielding zone, but did not experience a decrease in lateral load until the second 100% Δ_m cycle. During the 60% Δ_m step of test I-BRB2, a weld at the east column support fractured, causing a drop in lateral load thus impacting the frame's ability to resist load during the compression cycle due to moderate rocking of the east column base. Similar to the two in-plane tests, out-of-plane tests O-BRB3 [Fig. 5(c)] and O-BRB4 [Fig. 5(d)] failed in the second 100% Δ_m cycle due to weak axis buckling of the steel core. The third test (O-BRB3) completed this cycle and an additional half cycle before it was terminated; the fourth test (O-BRB4) completed all three 100% Δ_m cycles. All hysteresis curves are generally symmetric indicating effective energy dissipation. Some slip, due to movement within the joints occurs when the applied force is reversed; however, this type of slip is common in systems with dowel connections (Xiong and Liu 2014; Dong et al. 2020; Williamson et al. 2023).

The lateral force versus drift ratio envelope for each test is defined by the lateral force and drift ratio corresponding to the peak force in the first cycle of each step. The achieved peak force between tests decreased as testing progressed due to minimal damage to the timber adjacent to the dowels. The average decrease in maximum lateral load between bare frame tests was 11% thus justifying the continued use of the frame. The TBRBFs were able to reach an average of 2.8% drift ratio in the positive (east) direction and 2.6% drift ratio in the negative (west) direction, as shown in the lateral force versus drift ratio envelopes of Fig. 5(e). The bare frame tests,

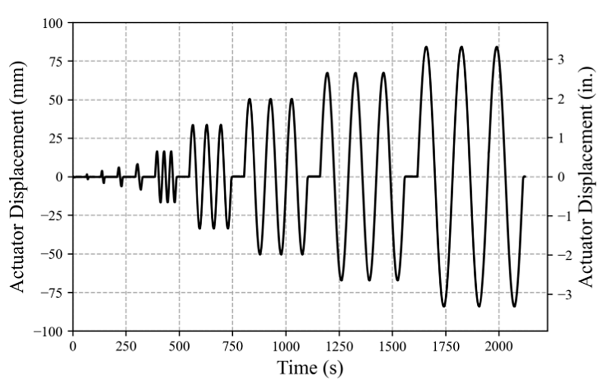

Step	Cycles	$\%\Delta_m$	Actuator Displacement mm (in.)
1	1	1.25	1 (0.04)
2	1	2.5	2 (0.08)
3	1	5	4 (0.17)
4	1	7.5	6 (0.25)
5	1	10	8 (0.33)
6	3	20	17 (0.66)
7	3	40	34 (1.32)
8	3	60	50 (1.98)
9	3	80	67 (2.64)
10	3	100	84 (3.30)

Fig. 3. ASTM E2126 cyclic loading protocol for timber components.

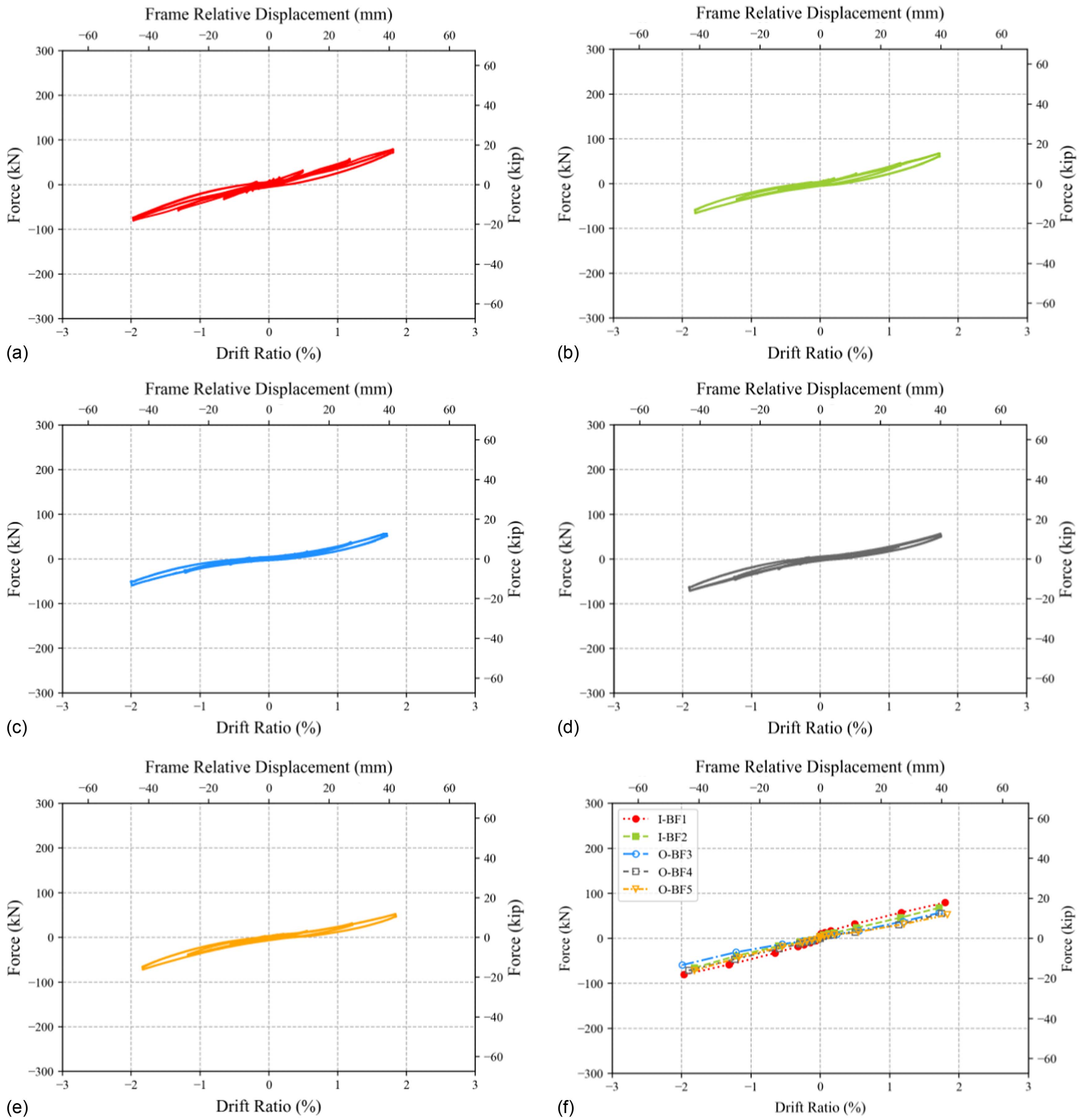

Fig. 4. Bare frame hysteresis curves: (a) I-BF1; (b) I-BF2; (c) O-BF3; (d) O-BF4; (e) O-BF5; and (f) bare frames hysteresis envelope.

subjected to drift ratios up to 2.0%, remained mostly linear elastic as shown in the envelopes of Fig. 4(f).

Out-of-Plane Displacement

An intentional out-of-plane displacement was imposed on the mass timber frame for tests O-BF3, O-BRB3, O-BF4, O-BRB4, and O-BF5 by wrapping a nylon strap around the top beam near the east connection and tightening it with a ratchet chain anchored to the steel reaction frame until the top east joint of the frame was pulled 25 mm (1 in.) out-of-plane relative to the top west joint; this was done to simulate three-dimensional effects in actual buildings subjected to earthquakes. The top west joint, which was located adjacent to the hydraulic actuator, was left intact and was monitored to ensure no out-of-plane movement occurred at this location. The starting location of the east beam-column joint is indicated with a star in Fig. 6(a); during the bare frame tests, the top east joint remained approximately 25 mm (1 in.) out-of-plane (North-South displacement) throughout the loading protocol. In contrast, during the TBRBF tests, the additional force from the

J. Struct. Eng., 2023, 149(10): 04023131

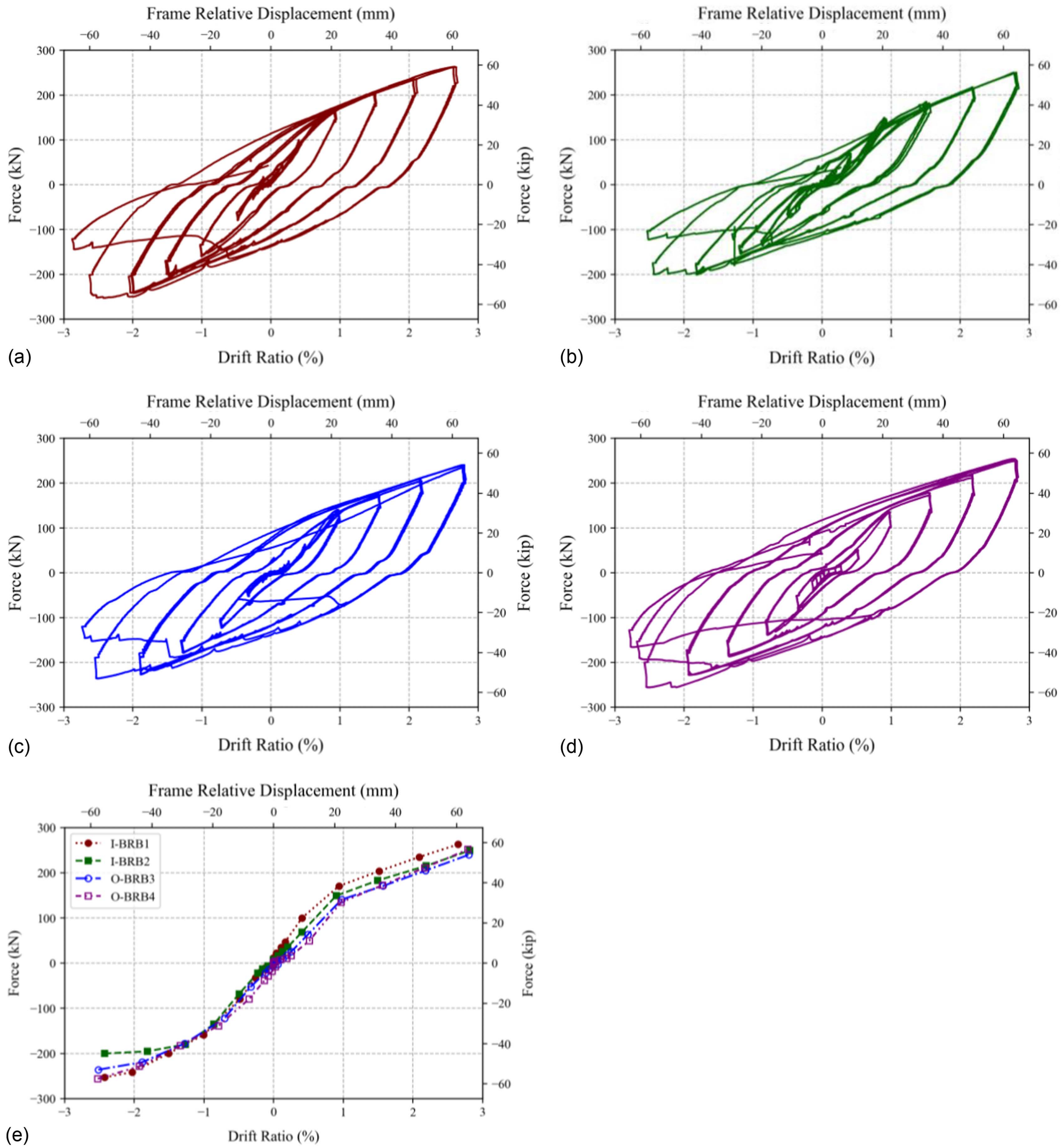

Fig. 5. TBRBF hysteresis curves: (a) I-BRB1; (b) I-BRB2; (c) O-BRB3; (d) O-BRB4; and (e) TBRBFs hysteresis envelope.

brace caused the out-of-plane displacement to increase to almost 51 mm (2.0 in.) at the peak positive drift, as shown in Fig. 6(b); during the compression cycle, the out-of-plane displacement decreased to 20 mm (0.8 in.), which could be caused by eccentric installation of the brace or by the northern tilt of the frame in the initial fit-up of the connections.

Column Axial Load

The total axial force applied to the columns [Figs. 6(c–f)] for each TBRBF test was determined by adding the force measured by the load cells of the two all-threaded bars per column. The maximum force in each all-threaded bar stayed below the 454 kN (102 kip) yield force. For the tests with 120 kN (27 kip) axial force, the maximum increase in axial load was 84% and the maximum decrease was 48%; for the tests with 300 kN (67.5 kip) axial force, the maximum increase was 103% and the maximum decrease 32%.

Displacement Ductility

The yield point for the TBRBF was estimated using the Yasumura and Kwai method (1998). The yield strength and displacement,

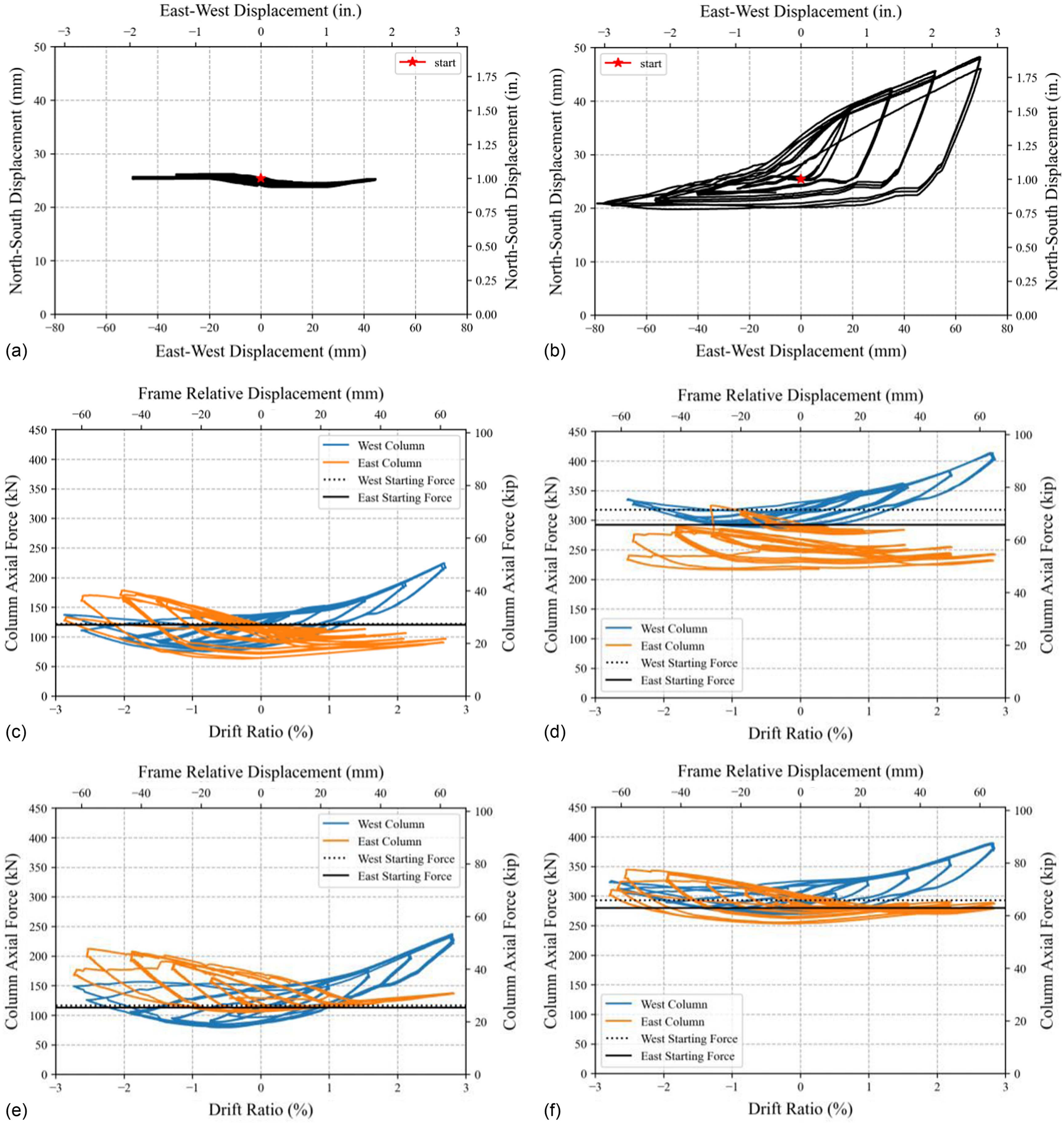

Fig. 6. Out-of-plane displacement of east column and total column axial forces: (a) east column displacement of O-BF4; (b) east column displacement of O-BRB4; (c) axial forces of I-BRB1; (d) axial forces of I-BRB2; (e) axial forces of O-BRB3; and (f) axial forces of O-BRB4.

maximum strength and displacement, and displacement ductility for the four TBRBF tests are provided in Table 3. When compared to other yield point estimation methods, this method was determined to be reliable even for connections with a lower initial stiffness (Muñoz et al. 2008). The maximum lateral force and maximum drift ratio were defined by the peak force at the first cycle of the step in which the TBRB failed. The maximum displacement ductility using the Yasumura and Kwai (1998) method ranged from 3.1 to 3.5.

To compare the results to existing research, the displacement ductility was determined using the EEEP method (ASTM 2011). The maximum displacement ductility determined by the EEEP method ranged from 2.1 to 2.9; these values are comparable to the ones presented by Dong et al. (2020) with conventional BRBs for a ductility of 2.3 to 2.8. The ductility of the TBRBFs in this research is double the ductility found for timber frames with conventional timber braces using X-brace and K-brace configurations (Xiong and Liu 2014). The tests carried out in this research

Table 3. Strength and ductility properties of TBRBFs

Test	Direction	Yield strength [kN (kip)]	Yield relative displacement[a] [mm (in.)]	Maximum strength [kN (kip)]	Maximum relative displacement[a] [mm (in.)]	Displacement ductility (Y&K method)
I-BRB1	Positive	148.3 (33.3)	17.6 (0.7)	262.7 (59.1)	60.6 (2.4)	3.4
	Negative	141.9 (31.9)	20.4 (0.8)	253.0 (56.9)	55.4 (2.2)	2.7
I-BRB2	Positive	149.8 (33.7)	20.8 (0.8)	249.4 (56.1)	64.4 (2.5)	3.1
	Negative	147.9 (33.2)	22.3 (0.9)	200.1 (45.0)	55.4 (2.2)	2.5
O-BRB3	Positive	140.5 (31.6)	22.3 (0.9)	239.9 (53.9)	64.1 (2.5)	2.9
	Negative	126.0 (28.3)	16.9 (0.7)	236.0 (53.1)	57.5 (2.3)	3.4
O-BRB4	Positive	138.0 (31.0)	23.4 (0.9)	251.5 (56.5)	63.8 (2.5)	2.7
	Negative	127.7 (28.7)	16.2 (0.6)	256.1 (57.6)	57.7 (2.3)	3.5

[a]Relative displacement is the difference in displacement between the top and bottom beam centerlines.

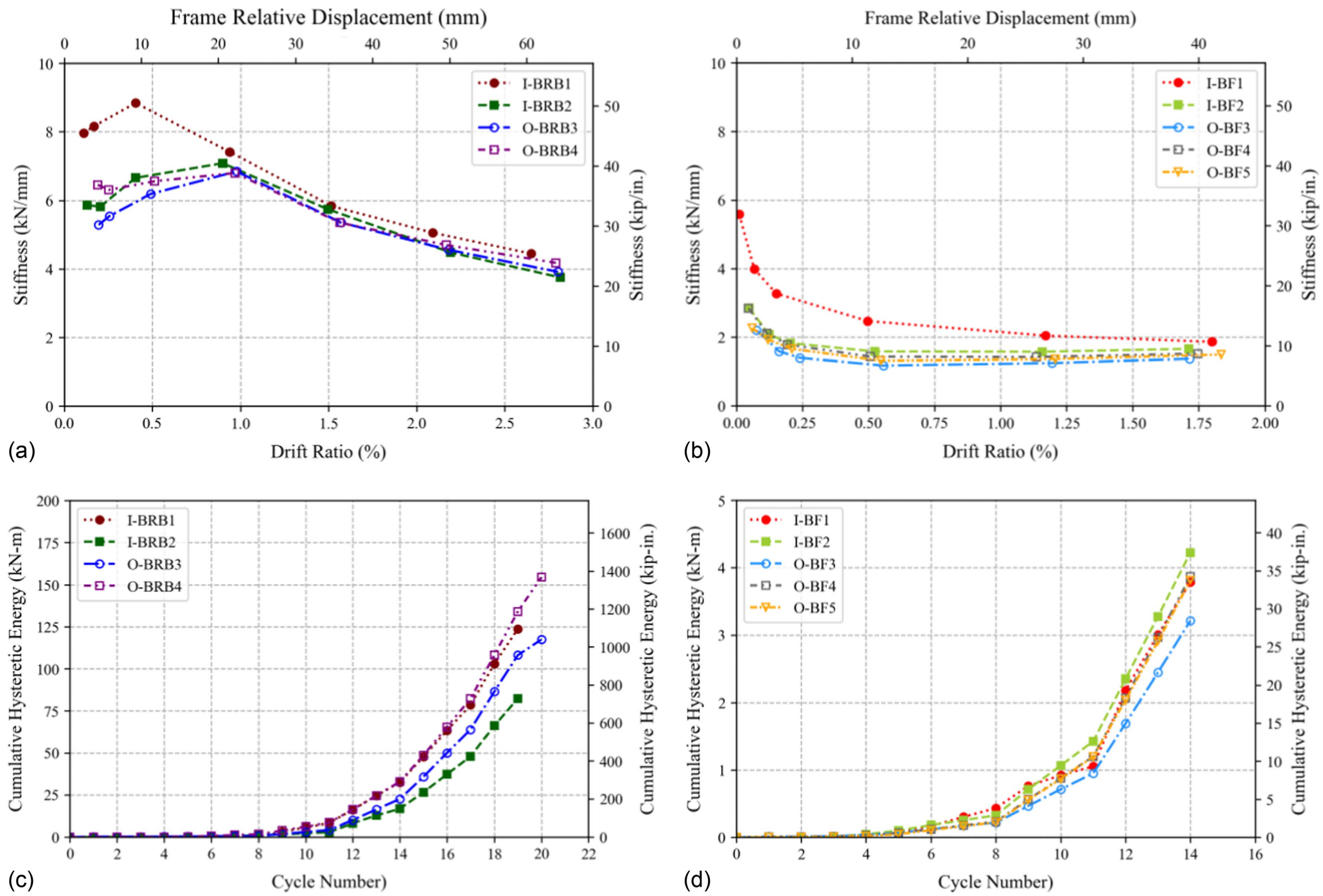

Fig. 7. Secant stiffness and cumulative hysteretic energy dissipation: (a) stiffness of TBRB frames; (b) stiffness of bare frames; (c) hysteretic energy of TBRB frames; and (d) hysteretic energy of bare frames.

included in-plane and out-of-plane tests while previous tests were performed only in-plane (Dong et al. 2020; Xiong and Liu 2014).

Stiffness Degradation

The secant stiffness degradation was calculated for the TBRBF subassemblies [Fig. 7(a)] and the bare mass timber frames [Fig. 7(b)] using Eq. (3):

$$k_i = \frac{|F_i^+| + |F_i^-|}{|X_i^+| + |X_i^-|} \tag{3}$$

where k_i = stiffness of cycle i; F_i^+ and F_i^- = peak forces in the positive and negative direction for the cycle; and X_i^+ and X_i^- = drift ratios corresponding to the peak forces. The initial stiffness decreased with each TBRBF test. The stiffness converges beyond a story drift ratio of 1.0%. In all TBRBF tests the peak stiffness occurred once the TBRB was able to fully engage. The bare frame tests achieved the highest stiffness at the beginning of the first test (I-BF1). There is little difference between the stiffness in the last three bare frame tests since the timber had already been crushed by dowels in the beam-column joint area; so when the loading protocol was repeated, only the steel dowels were contributing significantly to the stiffness. The stiffness of the bare frame is relatively low because the connections provide limited bending moment resistance. The contribution of the TBRB to the stiffness of the subassembly is illustrated by showing the higher stiffness of the TBRBFs [Fig. 7(a)], as compared to the bare frame [Fig. 7(b)]. For example, the first bare frame test (I-BF1) started with a stiffness of 5.5 kN/mm (31.9 kip/in.) compared to the corresponding TBRB frame test (I-BRB1), which started at 8.0 kN/mm (45.4 kip/in.).

Hysteretic Energy

The cumulative hysteretic energy for each TBRB frame and for the bare frame is shown in Figs. 7(c and d), respectively. The out-of-plane TBRBF test with high axial load (O-BRB4) dissipated the highest hysteretic energy since it was subjected to the entire loading protocol, while the remaining tests were terminated early due to failure of the TBRB. Comparison of the hysteretic energy for the TBRBF and the bare frame demonstrates the advantage of using the TBRBF as the lateral force resisting system. For example, at the end of cycle 14 for test O-BRB3, the system dissipated approximately 25 kN-m (221 kip-in.) compared to approximately 3 kN-m (27 kip-in.) for test O-BF3 after completion of the same number of cycles. After 14 cycles of lateral displacement the TBRB increased the energy dissipation of the system by 4.0 to 8.6 times compared to the bare frame.

Beam-Column Joint Rotations

Joint rotation was determined using LVDT measurements at the top and bottom of each beam-column joint and the relative distance between them. In general, the joint rotation for the TBRBF tests remained below 0.036 rad (2.1°) and was symmetric between the east and west sides of the frame, as shown in Figs. 8(a–d); the joints on both sides of the frame reached higher rotations during positive drift ratios. The joint rotation for the bare frame tests remained below 0.024 rad (1.4°) and was also symmetric between the east and west sides of the frame. Crushing of timber and movement of the west column base on the roller support contributed to the total maximum drift. Despite the fact that the joints were contributing to the drift, the steel dowels remained elastic and were not replaced between tests.

Timber BRB Performance

The TBRB continued to resist forces after initial splitting of the timber casing had initiated. Although the brace was not able to develop the same strength in compression after the casing started to split, it was able to continue dissipating hysteretic energy. When the brace went into the tension phase of the cycle following the start of MPP splitting, the gap was closed since the buckled steel core was stretched out again in tension.

Coupon tests of the steel cores showed that the steel yield stress was 262 MPa (38 ksi); therefore, the true yield force of the TBRB was 169 kN (38 kips). The strain in the TBRB steel core measured by LVDTs for I-BRB1 [Fig. 8(e)] and O-BRB3 [Fig. 8(f)] indicates that straining of the TBRB contributes to the drift achieved by the entire system. The average ratio of achieved maximum strain divided by the yield strain was 14.0 for test I-BRB1 and 15.5 for O-BRB3; these are representative strains for well-performing BRBs. These strain ratios exceed the design limit of 13.3 for conventional BRBs in ASCE 41-17 (ASCE 2017). However, the strains achieved by the TBRBs in these tests remained relatively low which prevented the full effects of strain hardening to develop in compression; this fact allowed the lateral forces in the positive and negative direction to be of similar magnitude.

Gusset plate strains for the third TBRBF test (O-BRB3), which is representative of the results for all TBRBF tests, reached a maximum of 0.30 times the yield strain in compression and 0.10 times the yield strain in tension at the east gusset plate (top). The west gusset plate (bottom) achieved a maximum strain of 0.04 times the yield in compression and 0.03 times the yield in tension. The larger values of strain for the east gusset plate (top) were expected because that gusset was in a more fixed condition within the beam-column joint compared to the west gusset plate; this is the case since the west column base, which is near the beam-column-brace connection, was allowed to displace on the rollers and this helped reduce the demand on that gusset plate (bottom).

Postexperiment Observations

Frame and Connections

Throughout the tests there was no visible external damage to the timber. Following completion of the tests, the joints were dissected to observe any internal damage [Figs. 9(a and b)]. Essentially no damage to the steel plates and surrounding timber was observed and little-to-no bending of the steel dowels. This, along with the relatively small rotations measured during the tests of 0.036 rad (2.1°) [Figs. 8(a–d)] compared to their capacity of 0.11 rad (6.3°) (Williamson et al. 2023), suggests that the frame remained mostly linear elastic for all the tests.

TBRBs

The elongation of the steel core during the largest cycle of test O-BRB3 is shown in Fig. 9(c); the first silver line indicates where the end of the casing was before testing began. After each TBRBF test was completed, the TBRB was deconstructed to observe the failure mode of the steel core. Each TBRB experienced weak axis buckling of the steel core [Fig. 9(d)]. Tests O-BRB3 and O-BRB4 developed waves with a maximum amplitude of 64 mm (2.5 in.) and 51 mm (2.0 in.), respectively; this is larger than the maximum amplitude of 41 mm (1.6 in.) and 33 mm (1.3 in.) developed in test I-BRB1 and I-BRB2, respectively. The weak axis buckling of the steel core occurred because the MPP casing is relatively soft and can be deformed by the steel. To mitigate this deformation, the hardness of the casing could be reinforced with another material such as stiffer MPP layers in the core region, steel side plates between the core and the timber casing or screw reinforcing. The largest amplitude wave occurred at the end of the yielding region and caused the MPP casing to crush and split between the plies [Figs. 9(e–h)]. Splitting always started near the end of the casing, where the largest amplitude wave of the steel core was located, and propagated along the casing length as the compression displacement increased. Failure at the end of the yielding zone could be due to bending moment at the TBRB ends, which was not accounted for in the design, from the eccentric brace installation, or the natural tilt of the frame.

Practical Application Discussion

The experimental findings show promising results for the performance of the TBRBF as a timber lateral force resisting system. The frame performed effectively during all nine tests with no visible external damage to the beam-column joints and no permanent bending to the steel dowels. Moreover, the repeated use of the timber frame throughout the testing program demonstrated that

J. Struct. Eng., 2023, 149(10): 04023131

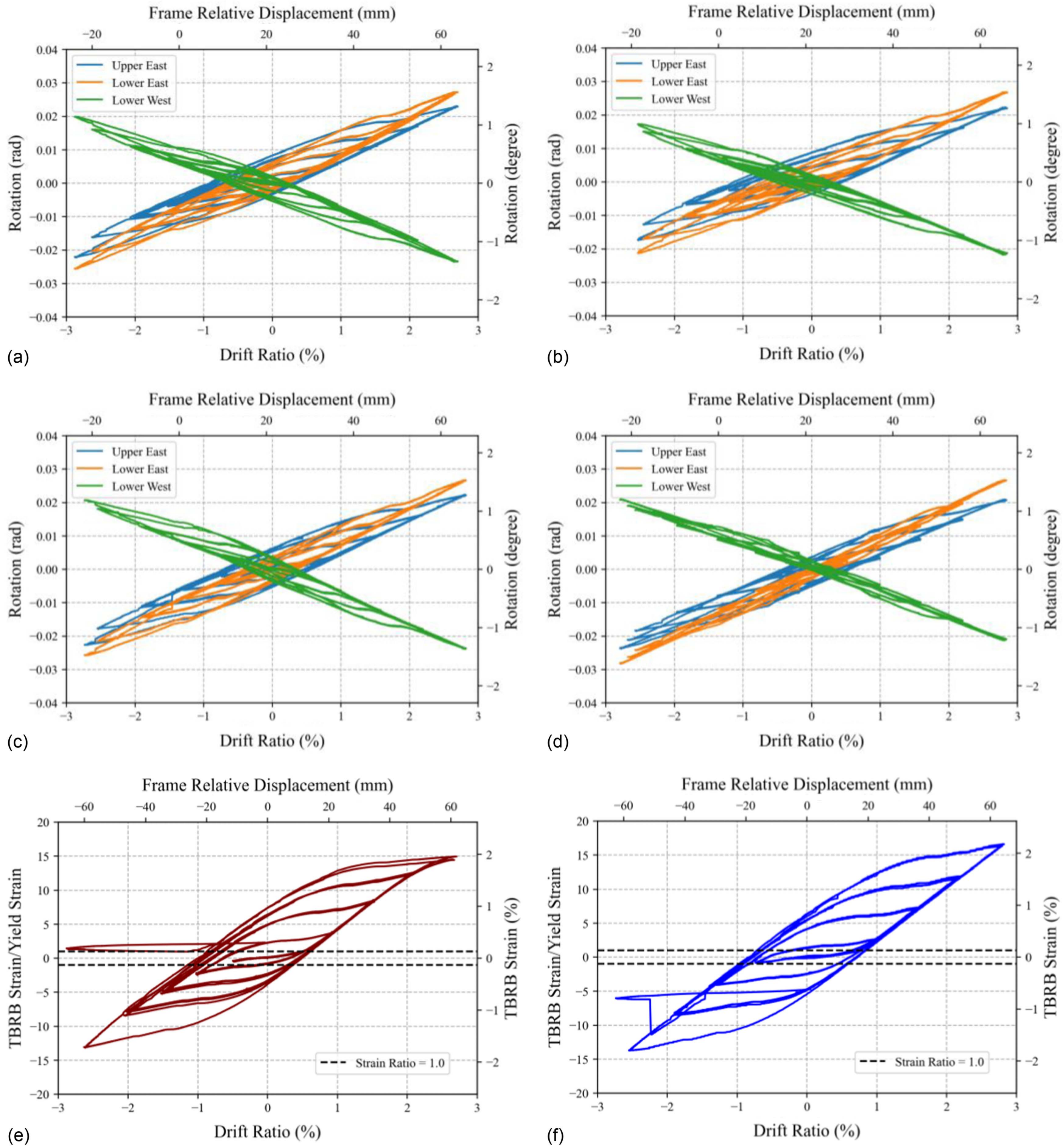

Fig. 8. TBRBF joint rotations and TBRB strains: (a) rotation for I-BRB1; (b) I-BRB2 rotation; (c) O-BRB3 rotation; (d) O-BRB4 rotation; (e) strain in TBRB for I-BRB1; and (f) strain in TBRB for O-BRB3.

the TBRBs can be replaced following an earthquake without compromising the integrity of the timber frame. The strains achieved in the TBRB show that it can meet the requirements for conventional BRBs, although further testing of TBRBFs is desirable using the standard AISC 341-16 (AISC 2016) loading protocol. Furthermore, the results from full-scale TBRB component tests (Murphy et al. 2021) indicate that the TBRB is capable of satisfying the requirements set by AISC 341-16 (AISC 2016). Hence, it is likely that a full-scale TBRBF would perform satisfactorily. Full-scale building shake table tests of TBRBFs under simulated earthquakes should also be carried out to confirm the findings of this study.

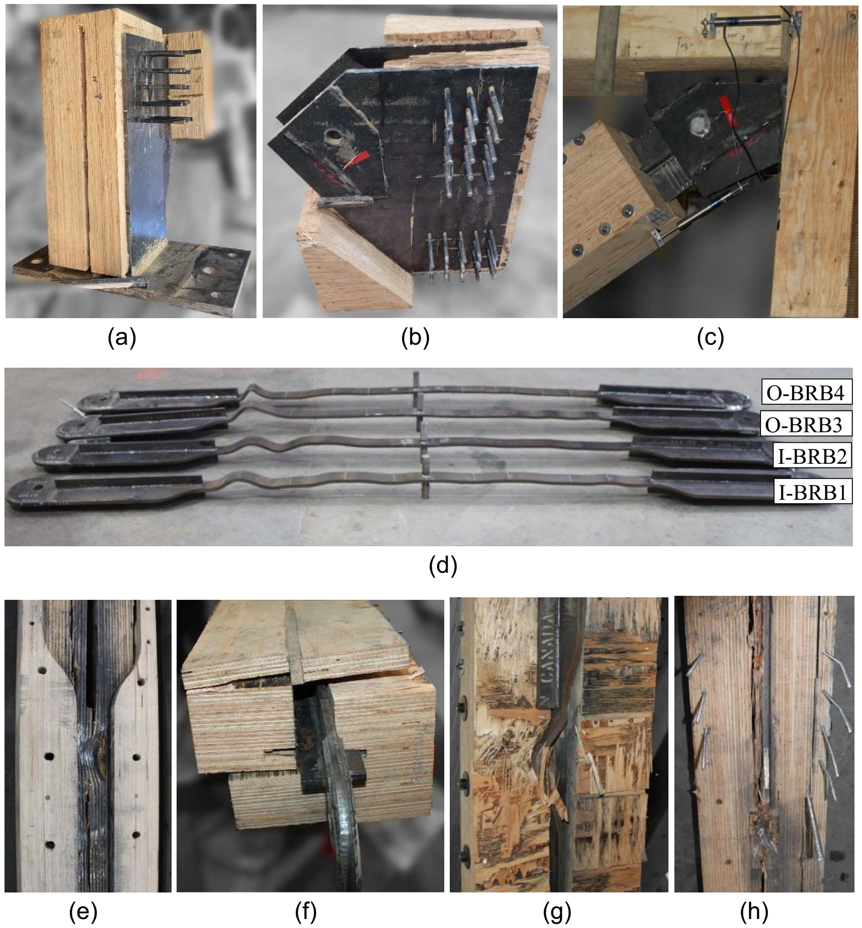

Fig. 9. Post-test condition of TBRBFs: (a) bottom east joint; (b) top east joint; (c) elongation of steel core for O-BRB3; (d) steel cores of TBRBs; (e) casing for I-BRB1; (f) casing for I-BRB2; (g) casing for O-BRB3; and (h) casing for O-BRB4.

Conclusions

This research has investigated the performance of mass timber frames with or without a TBRB under quasi-static cyclic loads. Both in-plane and out-of-plane tests of TBRB frames were carried out. Based on the experiments of the bare timber frames and the TBRBFs, the following conclusions can be drawn:

1. The four TBRBFs were able to achieve similar forces and drift capacities in both tension and compression. All of the hysteresis curves were generally symmetric and the loops were stable, indicating effective hysteretic energy dissipation, even in the case of the system with out-of-plane displacement.
2. All TBRBFs completed at least two full cycles of the 100% Δ_m step in the ASTM E2126 loading protocol for cyclic tests of timber components, and one test completed all three cycles of the 100% Δ_m step.
3. The maximum strain in the TBRB steel cores for all TBRBF tests ranged from 15.0 to 17.0 times the yield strain in tension and 8.0 to 14.0 times the yield strain in compression; these strains are within the expected range of well-performing BRBs.
4. The steel gusset plates performed well for both in-plane and out-of-plane TBRBF tests. The strain in the gusset plates reached a maximum of 0.30 times the yield strain in compression and 0.10 times the yield strain in tension.
5. The maximum displacement ductility determined using the Y&K method for both the in-plane and out-of-plane TBRBF tests ranged from 3.1 to 3.5. Using the EEEP method, the maximum displacement ductility ranged from 2.1 to 2.9, which is comparable to mass timber frame tests using conventional BRBs. The displacement ductility of the TBRBF tests is double the ductility of conventional timber braced frames.
6. The rotations at the beam-column connections of the TBRBFs remained below 0.036 rad (2.1°) and were symmetric between the east and west sides of the frame for both in-plane and out-of-plane tests. No damage to the connection steel plates and surrounding timber was observed and negligible bending of the steel dowels; this fact, and the relatively small rotations measured compared to their capacity, suggests that the frame remained linear elastic throughout the tests.
7. The bare mass timber frame tests were terminated at a drift ratio of 2.0% to ensure that the timber frame remained linear elastic, which was confirmed in the experiments.
8. The stiffness of the bare mass timber frame was significantly less than that of the TBRBF since the beam-column joints provided limited bending moment resistance.
9. The TBRB increased the cumulative hysteretic energy dissipation by 4.0 to 8.6 times compared to the bare timber frame after 14 cycles. At 2.0% drift ratio, the TBRB increased the lateral load capacity of the bare timber frame by a factor of 3.0 to 3.8.

Data Availability Statement

Some or all data, models or code that supports the findings of this study are available from the corresponding author upon reasonable request.

Acknowledgments

The authors would like to acknowledge the financial support provided by Wood Innovations, under USDA Grant No. 20-DG-11046000-615. The authors also acknowledge the donation of materials by Freres Lumber Co., Inc., and CoreBrace LLC. The authors acknowledge the in-kind timber modeling and CNC fabrication assistance provided by Timberlab. The authors acknowledge the assistance of M. Bryant, D. Tran, D. Briggs, S. Neupane, and S. Shrestha of the University of Utah for their assistance in carrying out the experiments.

References

AISC. 2016. *Seismic provisions for structural steel buildings*. ANSI/AISC 341-16. Chicago: AISC.

APA (The Engineered Wood Association). 2022. *Freres mass ply panels (MPP), and mass ply lam (MPL) beams and columns*. Tacoma, WA: Freres Lumber Co., Inc.

ASCE. 2017. *Seismic evaluation and retrofit of existing buildings*. ASCE/SEI 41-17. Reston, VA: ASCE.

ASTM. 2011. *Standard test methods for cyclic (reversed) load test for shear resistance of vertical elements of the lateral force resisting system for buildings*. ASTM E2126. West Conshohocken, PA: ASTM.

ASTM. 2019. *Standard specification for evaluation of structural composite lumber products*. ASTM D5456. West Conshohocken, PA: ASTM.

AWC (American Wood Council). 2018a. *National design specification for wood construction*. Leesburg, VA: AWC.

AWC (American Wood Council). 2018b. *Technical report 12: General dowel equations for calculating lateral connection values with appendix A*. Leesburg, VA: AWC.

Black, C. J., N. Makris, and I. D. Aiken. 2004. "Component testing, seismic evaluation and characterization of BRBs." *J. Struct. Eng.* 130 (6): 880–894. https://doi.org/10.1061/(ASCE)0733-9445(2004)130:6(880).

Busch, A., R. B. Zimmerman, S. Pei, E. McDonnell, P. Line, and D. Huang. 2021. "Prescriptive seismic design procedure for post-tensioned mass timber rocking walls." *J. Struct. Eng.* 148 (3): 04021289. https://doi.org/10.1061/(ASCE)ST.1943-541X.0003240.

Cao, J., H. Xiong, and Y. Cui. 2021. "Seismic performance analysis of timber frames based on a calibrated simplified model." *J. Build. Eng.* 46 (Apr): 103701. https://doi.org/10.1016/j.jobe.2021.103701.

Daneshvar, H., J. Niederwestberg, C. Dicof, R. Jackson, and Y. H. Chui. 2022a. "Perforated steel structural fuses in mass timber lateral load resisting system." *Eng. Struct.* 257 (Apr): 114097. https://doi.org/10.1016/j.entstruct.2022.114097.

Daneshvar, H., J. Niederwestberg, J. P. Letarte, and Y. H. Chui. 2022b. "Yield mechanisms of base shear connections for cross-laminated timber shear walls." *Constr. Build. Mater.* 335 (Jun): 127498. https://doi.org/10.1016/j.conbuildmat.2022.127498.

Dietsch, P., and R. Brander. 2015. "Self-tapping screws and threaded rods as reinforcement for structural timber elements—A state-of-the-art report." *Constr. Build. Mater.* 97 (Oct): 78–89. https://doi.org/10.1016/j.conbuildmat.2015.04.028.

Dong, W., M. Li, M. He, and Z. Li. 2021. "Experimental testing and analytical modeling of glulam moment connections with self-drilling dowels." *J. Struct. Eng.* 147 (5): 04021047. https://doi.org/10.1061/(ASCE)ST.1943-541X.0002977.

Dong, W., M. Li, C. Lee, G. MacRae, and A. Abu. 2020. "Experimental testing of full-scale glulam frames with buckling restrained braces." *Eng. Struct.* 222 (Nov): 111081. https://doi.org/10.1016/j.engstruct.2020.111081.

Fahnestock, L. A., R. Sause, and J. M. Ricles. 2007. "Seismic response and performance of buckling-restrained braced frames." *J. Struct. Eng.* 133 (9): 1195–1204. https://doi.org/10.1061/(ASCE)0733-9445(2007)133:9(1195).

Fan, X., S. Zhang, and W. Qu. 2011. "Load-carrying behaviour of dowel-type timber connections with slotted-in steel plates." *Appl. Mech. Mater.* 94 (8): 43–47. https://doi.org/10.4028/www.scientific.net/AMM.94-96.43.

Fitzgerald, D., T. H. Miller, A. Sinha, and J. A. Nairn. 2020. "Cross-laminated timber rocking walls with slip-friction connections." *Eng. Struct.* 220 (Oct): 110973. https://doi.org/10.1016/j.engstruct.2020.110973.

Ganey, R., J. Berman, T. Akbas, S. Loftus, J. D. Dolan, R. Sause, J. Ricles, S. Pei, J. van de Lindt, and H.-E. Blomgren. 2017. "Experimental investigation of self-centering cross-laminated timber walls." *J. Struct. Eng.* 143 (10): 04017135. https://doi.org/10.1061/(ASCE)ST.1943-541X.0001877.

Gilbert, C. F., and J. Erochko. 2019. "Development and testing of hybrid timber-steel braced frames." *Eng. Struct.* 198 (Nov): 109495. https://doi.org/10.1016/j.engstruct.2019.109495.

Hashemi, A., S. M. M. Yousef-Beik, P. Zarnani, and P. Quenneville. 2021. "Seismic strengthening of conventional timber structures using resilient braces." *Structures* 32 (Aug): 1619–1633. https://doi.org/10.1016/j.istruc.2021.03.100.

Hashemi, A., P. Zarnani, R. Masoudina, and P. Quennneville. 2017. "Experimental testing of rocking cross-laminated timber walls with resilient slip friction joints." *J. Struct. Eng.* 144 (1): 04017180. https://doi.org/10.1061/(ASCE)ST.1943-541X.0001931.

ICC (International Code Council). 2021. *International building code*. Falls Church, VA: International Building Code.

Lo Ricco, M., D. R. Rammer, M. O. Amini, A. Ghorbanpoor, P. Shiling, and R. B. Zimmerman. 2021. "Equivalent lateral force procedure for a building with a self-centering rocking story of cross-laminated timber (CLT) walls." In *Proc., World Conf. on Timber Engineering*. Red Hook, NY: Curran Associates.

Min-juan, H., and L. Hui-fen. 2015. "Comparison of glulam post-to-beam connections reinforced by two different dowel-type fasteners." *Constr. Build. Mater.* 99 (Nov): 99–108. https://doi.org/10.1016/j.conbuildmat.2015.09.005.

Morrell, I., R. Soti, B. Miyamoto, and A. Sinha. 2020. "Experimental investigation of base conditions affecting seismic performance of mass plywood panel shear walls." *J. Struct. Eng.* 146 (8): 04020149. https://doi.org/10.1061/(ASCE)ST.1943-541X.0002674.

Muñoz, W., M. Mohammad, A. Salenikovich, and P. Quenneville. 2008. *Determination of yield point and ductility of timber assemblies: In search for a harmonized approach*. Tacoma, WA: Engineered Wood Products Association.

Murphy, C., C. P. Pantelides, H.-E. Blomgren, and D. Rammer. 2021. "Development of timber buckling restrained brace for mass timber-braced frames." *J. Struct. Eng.* 147 (5): 04021050. https://doi.org/10.1061/(ASCE)ST.1943-541X.0002996.

Otero-Chans, D., J. Estévez-Cimadevila, F. Suárez-Riestra, and E. Martín-Gutiérrez. 2018. "Experimental analysis of glued-in steel plates used as shear connectors in timber-concrete-composites." *Eng. Struct.* 170 (Sep): 1–10. https://doi.org/10.1016/j.engstruct.2018.05.062.

Pei, S., J. W. van de Lindt, A. R. Barbosa, J. W. Berman, E. McDonnell, J. D. Dolan, H.-E. Blomgren, R. B. Zimmerman, D. Huang, and S. Wichman. 2019. "Experimental seismic response of a resilient 2-story mass-timber building with post-tensioned rocking walls." *J. Struct. Eng.* 145 (11): 04019120. https://doi.org/10.1061/(ASCE)ST.1943-541X.0002382.

Popovski, M., and I. Gavric. 2015. "Performance of a 2-story CLT house subjected to lateral loads." *J. Struct. Eng.* 142 (4): E4015006. https://doi.org/10.1061/(ASCE)ST.1943-541X.0001315.

Popovski, M., H. G. L. Prion, and E. Karacabeyli. 2001. "Seismic performance of connections in heavy timber construction." *Can. J. Civ. Eng.* 29 (3): 389–399. https://doi.org/10.1139/l02-020.

Popovski, M., H. G. L. Prion, and E. Karacabeyli. 2003. "Shake table tests on single-storey braced timber frames." *Can. J. Civ. Eng.* 30 (6): 1089–1100. https://doi.org/10.1139/l03-060.

Steiger, R., E. Serrano, M. Stepinac, V. Rajcic, C. O'Niell, D. McPolin, and R. Widmann. 2015. "Strengthening of timber structures with glued-in rods." *Constr. Build. Mater.* 97 (Oct): 90–105. https://doi.org/10.1016/j.conbuildmat.2015.03.097.

van de Lindt, J., M. O. Amini, D. Rammer, P. Line, S. Pei, and M. Popovski. 2020. "Seismic performance for cross-laminated timber shear wall systems in the United States." *J. Struct. Eng.* 146 (9): 04020172. https://doi.org/10.1061/(ASCE)ST.1943-541X.0002718.

van de Lindt, J., M. O. Amini, D. Rammer, P. Line, S. Pei, and M. Popovski. 2022. *Determination of seismic performance factors for cross-laminated timber shear walls based on FEMA P695 methodology. General Technical Report FPL-GTR-281*. Madison, WI: US Department of Agriculture, Forest Service, Forest Products Laboratory.

Williamson, E., C. P. Pantelides, H.-E. Blomgren, and D. Rammer. 2023. "Performance of beam-column connections with Mass Ply Lam and steel dowels under cyclic loads." *J. Struct. Eng.* 149 (6): 04023057. https://doi.org/10.1061/JSENDH.STENG-11569.

Wu, A.-C., P.-C. Lin, and K.-C. Tsai. 2014. "High-mode buckling responses of buckling-restrained brace core plates." *Earthquake Eng. Struct. Dyn.* 43 (3): 375–393. https://doi.org/10.1002/eqe.2349.

Xiong, H., and Y. Liu. 2014. "Experimental study of the lateral resistance of bolted glulam timber post and beam structural systems." *J. Struct. Eng.* 142 (4): E4014002. https://doi.org/10.1061/(ASCE)ST.1943-541X.0001205.

Xu, W., and C. P. Pantelides. 2017. "Strong-axis and weak-axis buckling and local bulging of buckling-restrained braces with prismatic core plates." *Eng. Struct.* 153 (Dec): 279–289. https://doi.org/10.1016/j.engstruct.2017.10.017.

Yasumura, M., and N. Kwai. 1998. "Estimating seismic performance of wood-frame structures." In *Proc., 5th World Conf. on Timber Engineering*, 564–571. Lausanne, Switzerland: Swiss Federal Institute of Technology.

Yousef-beik, S. M. M., A. Hashemi, S. Veismoradi, and P. Quenneville. 2020. "Self-centering bracing system: Avoidance of elastic buckling for braces with one intermediate damper." In *Proc., New Zealand Society of Earthquake Engineering (NZSEE) Conf.* Wellington, New Zealand: New Zealand Society for Earthquake Engineering.

Zhang, C., H. Guo, K. Jung, R. Harris, and W.-H. Chang. 2019. "Screw reinforcement on dowel-type moment-resisting connections with cracks." *Constr. Build. Mater.* 215 (Aug): 59–72. https://doi.org/10.1016/j.conbuildmat.2019.04.160.